

1 Last interglacial ocean changes in the Bahamas: climate 2 teleconnections between low and high latitudes

3
4 Anastasia Zhuravleva¹ and Henning A. Bauch²

5 ¹Academy of Sciences, Humanities and Literature, Mainz c/o GEOMAR Helmholtz Centre for Ocean Research,
6 Wischhofstrasse 1-3, Kiel, 24148, Germany

7
8 ²Alfred Wegener Institute, Helmholtz Centre for Polar and Marine Research c/o GEOMAR Helmholtz Centre for
9 Ocean Research, Wischhofstrasse 1-3, Kiel, 24148, Germany

10
11 *Correspondence to:* Anastasia Zhuravleva (azhuravleva@geomar.de)

12
13
14 **Abstract.** Paleorecords and modeling studies suggest that instabilities in the Atlantic Meridional Overturning
15 Circulation (AMOC) strongly affect the low-latitude climate, namely via feedbacks on the Atlantic Intertropical
16 Convergence Zone (ITCZ). Despite pronounced millennial-scale overturning and climatic variability documented
17 in the subpolar North Atlantic during the last interglacial period (MIS 5e), studies on the cross-latitude
18 teleconnections remain to be very limited, precluding full understanding of the mechanisms controlling
19 subtropical climate evolution across the last warm cycle. Here, we present new planktic foraminiferal assemblage
20 data combined with $\delta^{18}\text{O}$ values in surface and thermocline-dwelling foraminifera from the Bahama region, which
21 is ideally suited to study past changes in subtropical ocean and atmosphere. Our data reveal that the peak sea
22 surface warmth during early MIS 5e was intersected by an abrupt millennial-scale cooling/salinification event,
23 which was possibly associated with a sudden southward displacement of the mean annual ITCZ position. This
24 atmospheric shift is, in turn, ascribed to the transitional climatic regime of early MIS 5e, characterized by
25 persistent ocean freshening in the high latitudes and, therefore, an unstable AMOC mode.

28 **1 Introduction**

29 In the low-latitude North Atlantic, wind patterns, precipitation-evaporation balance as well as sea surface
30 temperatures (SSTs) and salinities (SSSs) are strongly dependent on the position of the Atlantic Intertropical
31 Convergence Zone (ITCZ) and its associated rainfall (Peterson and Haug, 2006). Based on paleorecords and
32 modelling studies, past positions of the ITCZ are thought to be related to the interhemispheric thermal contrast
33 (Schneider et al., 2014). In turn, changes in the thermal contrast could be principally driven by two mechanisms:
34 (1) precessional cycle and, associated with it, cross-latitudinal distribution of solar insolation, or (2) millennial-
35 scale climatic variability brought about by Atlantic Meridional Overturning Circulation (AMOC) instabilities
36 (Wang et al., 2004; Broccoli et al., 2006; Arbuszewski et al., 2013; Schneider et al., 2014). Specifically,
37 millennial-scale cold events in the high northern latitudes were linked with reduced convection rates of the
38 AMOC, accounting for both a decreased oceanic transport of the tropical heat towards the north and a southward
39 shift of the mean annual position of the ITCZ (Vellinga and Wood, 2002; Chiang et al., 2003; Broccoli et al.,
40 2006). Reconstructions from the low-latitude North Atlantic confirm southward displacements of the ITCZ coeval
41 with AMOC reductions and reveal a complex hydrographic response within the upper water column, generally
42 suggesting an accumulation of heat and salt in the (sub)tropics (Schmidt et al., 2006a; Carlson et al., 2008; Bahr
43 et al., 2011; 2013). There are, however, opposing views on the subtropical sea surface development at times of
44 high-latitude cooling events. While some studies suggest stable or increasing SSTs (Schmidt et al., 2006a; Bahr
45 et al., 2011; 2013), others imply an atmospheric-induced (evaporative) cooling (Chang et al., 2008; Chiang et al.,
46 2008).

47 The last interglacial (MIS 5e), lasting from about ~130 to 115 thousand years before present (hereafter [ka]), is
48 often referred to as a warmer-than-preindustrial interval (Hoffman et al., 2017), associated with significantly
49 reduced ice sheets and a sea level rise up to 6-9 meters above the present levels (Dutton et al., 2015). This time
50 period has attracted a lot of attention as a possible analog for future climatic development as well as a critical
51 target for validation of climatic models (Masson-Delmotte et al., 2013). Proxy data from the North Atlantic
52 demonstrate that the climate of the last interglacial was relatively unstable, involving one or several cooling events
53 (Maslin et al., 1998; Fronval and Jansen, 1997; Bauch et al., 2012; Irvál et al., 2012, 2016; Zhuravleva et al.,
54 2017a, b). This climatic variability is thought to be strongly related to changes in the AMOC strength (Adkins et
55 al., 1997). Thus, recent studies reveal that the AMOC abruptly recovered after MIS 6 deglaciation (Termination
56 2 or T2), i.e., at the onset of MIS 5e, at ~ 129 ka, but it was interrupted around 127-126 ka (Galaasen et al., 2014;
57 Deaney et al., 2017). Despite the pronounced millennial-scale climatic variability documented in the high northern

58 latitudes, studies on the cross-latitudinal links are very limited (but see e.g., Cortijo et al., 1999; Schwab et al.,
59 2013; Kandiano et al., 2014; Govin et al., 2015; Jiménez-Amat and Zahn, 2015). This precludes the full
60 understanding of the mechanisms (e.g., insolation, oceanic and/or atmospheric forcing versus high-to-low-
61 latitudes climate feedbacks), regulating subtropical climate across the last interglacial.
62 Given its critical location near the origin of the Gulf Stream, sediments from the slopes of the shallow-water
63 carbonate platforms of the Bahamian archipelago (Fig. 1) have been previously investigated in terms of oceanic
64 and atmospheric variability (Slowey and Curry, 1995; Roth and Reijmer, 2004; 2005; Chabaud et al., 2016).
65 However, a thorough study of the last interglacial climatic evolution underpinned by a critical stratigraphical
66 insight is lacking so far. Here, a sediment record from the Little Bahama Bank (LBB) region is investigated for
67 possible links between the AMOC variability and the ITCZ during the last interglacial cycle. Today the LBB
68 region lies at the northern edge of the influence of the Atlantic Warm Pool, which expansion is strongly related
69 to the ITCZ movements (Wang and Lee, 2007; Levitus et al., 2013), making our site particularly sensitive to
70 monitor past shifts of the ITCZ. Given that geochemical properties of marine sediments around carbonate
71 platforms vary in response to sea level fluctuations (e.g., Lantzsich et al., 2007), X-ray fluorescence (XRF) data
72 are being used together with stable isotope and faunal records to strengthen the temporal framework. Planktic
73 foraminiferal assemblage data complemented by $\delta^{18}\text{O}$ values, measured on surface- and thermocline-dwelling
74 foraminifera, are employed to reconstruct the upper ocean properties (stratification, trends in temperature and
75 salinity), specifically looking at mechanisms controlling the foraminiferal assemblages. Assuming a coupling
76 between foraminiferal assemblage data and past mean annual positions of the ITCZ (Poore et al., 2003; Vautravers
77 et al., 2007), our faunal records are then looked at in terms of potential geographical shifts of the ITCZ. Finally,
78 we compare our new proxy records with published evidence from the regions of deep water formation to draw
79 further conclusions on the subpolar forcing on the low-latitude climate during MIS 5e.

80

81 **2 Regional Setting**

82 **2.1 Hydrographic context**

83 Core MD99-2202 (27°34.5' N, 78°57.9' W, 460 m water depth) was taken from the upper northern slope of the
84 LBB, which is the northernmost shallow-water carbonate platform of the Bahamian archipelago. The study area
85 is at the western boundary of the wind-driven subtropical gyre (STG), in the vicinity to the Gulf Stream (Fig. 1a),
86 which supplies both heat and salt to the high northern latitudes thereby constituting the upper cell of the AMOC.

87 In the western subtropical North Atlantic two distinctly different layers can be distinguished within the upper 500
88 m of the water column (Fig. 1c). The uppermost mixed layer (upper 50-100 m) is occupied by warm and
89 comparatively fresh waters ($T > 24^{\circ}\text{C}$, $S < 36.4$ psu), predominantly coming from the equatorial Atlantic (Schmitz
90 and McCartney, 1993; Johns et al., 2002). Properties of this water mass vary significantly on seasonal timescales
91 and are closely related to the latitudinal migration of the ICTZ (Fig. 1b). During boreal winter (December-April),
92 when the ITCZ is in its southernmost position, the Bahama region is dominated by relatively cool, stormy weather
93 with prevailing northern and northeastern trade winds and is affected by cold western fronts, that increase
94 evaporation and vertical convective mixing (e.g., Wilson and Roberts, 1995). During May to November, as the
95 ITCZ moves northward, the LBB region is influenced by relatively weakened trade winds from the east and
96 southeast, increased precipitation and very warm waters of the Atlantic Warm Pool ($T > 28.5^{\circ}\text{C}$), which expand
97 into the Bahama region from the Caribbean Sea and the equatorial Atlantic (Stramma and Schott, 1999; Wang
98 and Lee, 2007; Levitus et al., 2013).

99 The mixed layer is underlain by the permanent thermocline, which is comprised of a homogeneous pool of
100 comparatively cool and salty ($T < 24^{\circ}\text{C}$, $S > 36.4$ psu) water (Schmitz and Richardson, 1991). These “mode” waters
101 are formed in the North Atlantic STG through wintertime subduction of surface waters generated by wind-driven
102 Ekman downwelling and buoyancy flux (Slowey and Curry, 1995).

103

104 **2.2 Sedimentological context**

105 Along the slopes of the LBB, sediments are composed of varying amounts of sedimentary input from the platform
106 top and from the open ocean, depending on the global sea level state (Droxler and Schlager, 1985; Schlager et al.,
107 1994). During interglacial highstands, when the platform top is submerged, the major source of sediment input is
108 the downslope transport of fine-grained aragonite needles, precipitated on the platform top. This material
109 incorporates significantly higher abundances of strontium (Sr), than found in pelagic-derived aragonite (e.g.,
110 pteropods) and calcite material from planktic foraminifera and coccoliths (Morse and MacKenzie, 1990). Given
111 that in the periplatform interglacial environment modifications of the aragonite content due to sea floor dissolution
112 and/or winnowing of fine-grained material are minimal (Droxler and Schlager, 1985; Schlager et al., 1994; Slowey
113 et al., 2002), thicker sediment packages accumulate on the slopes of the platform, yielding interglacial climate
114 records of high resolution (Roth and Reijmer, 2004; 2005). During glacial lowstands, on the contrary, as the LBB
115 bank top is exposed, aragonite production is limited, sedimentation rates are strongly reduced and coarser-grained

116 consolidated sediments are formed from the pelagic organisms (Droxler and Schlager, 1985; Slowey et al., 2002;
117 Lantzsch et al., 2007).

118

119 **3 Methods**

120 **3.1 Foraminiferal counts and stable isotope analyses**

121 Planktic foraminiferal assemblages were counted on representative splits of the 150-250 μm fraction containing
122 at least 300 individual specimens. Counts were also performed in the >250 μm fraction. The census data from the
123 two size fractions were added up and recalculated into relative abundance of planktic foraminifera in the fraction
124 >150 μm . Faunal data were obtained at each 2 cm for the core section between 508.5 and 244.5 cm and at each
125 10 cm between 240.5 and 150.5 cm. According to a standard practice, *Globorotalia menardii* and *Globorotalia*
126 *tumida* as well as *Globigerinoides sacculifer* and *Globigerinoides trilobus* were grouped together, and referred to
127 as *G. menardii* and *G. sacculifer*, respectively (Poore et al., 2003; Kandiano et al., 2012; Jentzen et al., 2018).

128 New oxygen isotope data were produced at 2 cm steps using ~ 10 -30 tests of *Globorotalia truncatulinoides* (dex)
129 and ~ 5 -20 tests of *Globorotalia inflata* for depths 508.5-244.5 cm and 508.5-420.5 cm, respectively. Analyses
130 were performed using a Finnigan MAT 253 mass spectrometer at the GEOMAR Stable Isotope Laboratory.
131 Calibration to the Vienna Pee Dee Belemnite (VPDB) isotope scale was made via the NBS-19 and an internal
132 laboratory standard. The analytical precision of in-house standards was better than 0.07 ‰ (1σ) for $\delta^{18}\text{O}$. Isotopic
133 data derived from the deep-dwelling foraminifera *G. truncatulinoides* (dex) and *G. inflata* could be largely
134 associated with the permanent thermocline and linked to winter conditions (Groeneveld and Chiessi, 2011;
135 Jonkers and Kučera, 2017; Jentzen et al., 2018). However, as calcification of their tests starts already in the mixed
136 layer and continues in the main thermocline (Fig. 1c), the abovementioned species are thought to accumulate in
137 their tests hydrographic signals from different water depths (Groeneveld and Chiessi, 2011; Mulitza et al., 1997).

138

139 **3.2 XRF scanning**

140 XRF analysis was performed in two different runs using the Aavatech XRF Core Scanner at Christian-Albrecht
141 University of Kiel (for technical details see Richter et al., 2006). To obtain intensities of elements with lower
142 atomic weight (e.g., calcium (Ca), chlorine (Cl)), XRF scanning measurements were carried out with the X-ray
143 tube voltage of 10 kv, the tube current of 750 μA and the counting time of 10 seconds. To analyze heavy elements
144 (e.g., iron (Fe), Sr), the X-ray generator setting of 30 kv and 2000 μA and the counting time of 20 seconds were
145 used; a palladium thick filter was placed in the X-ray tube to reduce the high background radiation generated by

146 the higher source energies. XRF Core Scanner data were collected directly from the split core sediment surface,
147 that had been flattened and covered with a 4 µm-thick ULTRALENE SPEXCerti Prep film to prevent
148 contamination of the measurement unit and desiccation of the sediment (Richter et al., 2006; Tjallingii et al.,
149 2007). The core section between 150 and 465 cm was scanned at 3 mm step size, whereas the coarser-grained
150 interval between 465 and 600 cm was analyzed at 10 mm resolution.

151 To account for potential biases related to physical properties of the sediment core (see e.g., Chabaud, 2016), XRF
152 intensities of Sr were normalized to Ca, the raw total counts of Fe and Sr were normalized to the total counts of
153 the 30 kv run; counts of Ca and Cl were normalized to the total counts of the 10 kv run, excluding rhodium
154 intensity, because this element intensities are biased by the signal generation (Bahr et al., 2014).

155

156 **4 Age model**

157 By using our foraminiferal assemblage data, we were able to refine the previously published age model of core
158 MD99-2202 (Lantsch et al., 2007). To correctly frame MIS 5e, stratigraphic subdivision of the unconsolidated
159 aragonite (Sr)-rich sediment package between 190 and 464 m is essential (Fig. 2). In agreement with Lantsch et
160 al. (2007), we interpret this core section to comprise MIS 5, which is supported by key biostratigraphic markers
161 used to identify the well-established faunal zones of late Quaternary (Ericson and Wollin, 1968). Thus, the last
162 occurrence of *G. menardii* at the end of the aragonite-rich sediment package is in agreement with the estimated
163 late MIS 5 age (ca. 80-90 ka; Boli and Saunders, 1985; Slowey et al., 2002; Bahr et al., 2011; Chabaud, 2016).

164 The coherent variability in the ~200-300 cm core interval, observed between aragonite content and relative
165 abundances of warm surface-dwelling foraminifera of *Globigerinoides* genus (*G. ruber*, white and pink varieties,
166 *G. conglobatus* and *G. sacculifer*), points to simultaneous climate and sea level-related changes and likely reflects
167 the warm/cold substages of MIS 5. The identified substages were then correlated with the global isotope benthic
168 stack LS16 (Lisiecki and Stern, 2016) using AnalySeries 2.0.8 (Paillard et al., 1996). Further, boundaries between
169 MIS 6/5e and 5e/5d as well as the penultimate glaciation (MIS 6) peak, defined from $\delta^{18}\text{O}$ record of *G. ruber*
170 (white), were aligned to the global benthic stack (Lisiecki and Stern, 2016).

171 Given that sedimentation rates at the glacial/interglacial transition could have changed drastically due to increased
172 production of Sr-rich aragonite material above the initially flooded carbonate platform top (Roth and Reijmer,
173 2004), we applied an additional age marker to better frame the onset of the MIS 5e “plateau” (Masson-Delmotte
174 et al., 2013) and to allow for a better core-to-core comparison. Thus, we tied the increased relative abundances of
175 warm surface-dwelling foraminifera of *Globigerinoides* genus, which coincides with the rapid decrease in

176 foraminiferal $\delta^{18}\text{O}$ record at 456 cm, with the onset of MIS 5e “plateau” at ~129 ka (Masson-Delmotte et al.,
177 2013). This age is in good agreement with many marine and speleothem records, dating a rapid post-stadial
178 warming and monsoon intensification to 129-128.7 ka (Govin et al., 2015; Jiménez-Amat and Zahn, 2015; Deaney
179 et al., 2017), coincident with the sharp methane increase in the EPICA Dome C ice core (Loulergue et al., 2008;
180 Govin et al., 2012). Although we do not apply a specific age marker to frame the decline of the MIS 5e “plateau”,
181 the resulting decrease in the percentage of warm surface-dwelling foraminifera of *Globigerinoides* genus as well
182 as the initial increase in the planktic $\delta^{18}\text{O}$ values dates back to ~117 ka (Figs. 3-5), which broadly coincides with
183 the cooling onset over Greenland (NGRIP community members, 2004). A similar subtropical-polar climatic
184 coupling was proposed in earlier studies from the western North Atlantic STG (e.g., Vautravers et al., 2004;
185 Schmidt et al., 2006a; Bahr et al., 2013; Deaney et al., 2017).

186

187 **5 Results**

188 **5.1 XRF data in the lithological context**

189 In Fig. 3, XRF-derived elemental data are plotted against lithological and sedimentological records. Beyond the
190 intervals with low Ca counts and correspondingly high Cl intensities (at 300-325 cm and 395-440 cm), Ca
191 intensities do not vary significantly, which is in line with a stable carbonate content of about 94 % wt, revealed
192 by Lantzsch et al. (2007). Our Sr record closely follows the aragonite curve, demonstrating that the interglacial
193 minerology is dominated by aragonite. Beyond the intervals containing reduced Ca intensities, a good coherence
194 between Sr/Ca and aragonite content is observed. The rapid increase in Sr/Ca and aragonite is found at the end of
195 the penultimate deglaciation (T2), coeval with the elevated absolute abundances of *G. menardii* per sample (Fig.
196 3). The gradual step-like Sr/Ca and aragonite decrease characterizes both the glacial inception and the later MIS
197 5 phase. Intensities of Fe abruptly decrease at the beginning of the last interglacial, but gradually increase during
198 the glacial inception (Fig. 4). Note that between ~112 and 114.5 ka, the actual XRF measurements were affected
199 by a low sediment level in the core tube.

200

201 **5.2 Climate-related proxies**

202 To calculate $\delta^{18}\text{O}$ gradients across the upper water column, we also used the published $\delta^{18}\text{O}$ data by Lantzsch et
203 al. (2007), which were measured on the surface-dwelling foraminifera *G. ruber* (white). These isotopic data can
204 be generally associated with mean annual conditions (Tedesco et al., 2007), however, during colder time intervals
205 productivity peak of *G. ruber* (white) could shift towards warmer months, leading to underestimation of the actual

206 environmental change (Schmidt et al., 2006a, b; Jonkers and Kučera, 2015). During the penultimate glacial
207 maximum (MIS 6), $\delta^{18}\text{O}$ gradients between *G. ruber* (white) and *G. truncatulinoides* (dex) and *G. inflata* are very
208 low (Fig. 4), succeeded by a gradually increasing difference across T2, ~135-129 ka. Changes in the isotopic
209 gradient between surface- and thermocline-dwelling foraminifera closely follow variations in the relative
210 abundances of *G. truncatulinoides* (dex) and *G. inflata* (Fig. 4). Across MIS 5e species of *Globigerinoides* genus
211 dominate the total assemblage, however, significant changes in the proportions of three main *Globigerinoides*
212 species are observed (Fig. 5): *G. sacculifer* and *G. ruber* (pink) essentially dominate the assemblage during early
213 MIS 5e (129-124 ka), whereas *G. ruber* (white) proportions are at their maximum during late MIS 5e (124-117
214 ka). At around 127 ka, all $\delta^{18}\text{O}$ records abruptly increase together with a reappearance of *G. inflata* (Fig. 4) and a
215 relative abundance decrease of *G. ruber* (pink) and *G. sacculifer* (Fig. 5). After 120 ka, $\delta^{18}\text{O}$ values in *G. ruber*
216 (white) and *G. truncatulinoides* (dex) become variable (Fig. 4). That instability coincides with an abrupt drop in
217 *G. sacculifer* relative abundances (Fig. 5).

218

219 **6 Discussion**

220 **6.1 Platform sedimentology and relative sea level change**

221 The modern LBB lagoon is shallow with an average water depth between 6-10 m (Williams, 1985). Despite some
222 possible isostatic subsidence of 1-2 m per hundred thousand years (Carew and Mylroie, 1995), the LBB region is
223 generally regarded as tectonically stable (Hearty and Neumann, 2001). Considering this, a relative sea level (RSL)
224 rise above -6 m of its present position is required to completely flood the platform top and allow for a drastic
225 increase in platform-derived (Sr-rich aragonite) sediment particles (Neumann and Land, 1975; Droxler and
226 Schlager, 1985; Schlager et al., 1994; Carew and Mylroie, 1997). As such, the LBB flooding periods exceeding -
227 6 m RSL can be defined from downcore variations in Sr/Ca intensity ratio (Chabaud et al., 2016).

228 While our Sr record likely represents a non-affected signal because of good coherence with the aragonite record,
229 some of the Ca intensity values are reduced due increased seawater content, as evidenced by simultaneously
230 measured elevated Cl intensities (Fig. 3). Because enhanced seawater content in the sediment appears to reduce
231 only Ca intensities, which leaves elements of higher atomic order (e.g., Fe, Sr) less affected (Tjallingii et al., 2007;
232 Hennekam and de Lange, 2012), normalization of Sr counts to Ca results in very high Sr/Ca intensity ratios across
233 the Cl-rich intervals. Regardless of these problematic intervals described above, the XRF-derived Sr/Ca values
234 agree well with the actually measured aragonite values that it seem permissible to interpret them in terms of RSL
235 variability. Here, it should be noted that, although the Bahama region is located quite far from the former

236 Laurentide Ice Sheet, there still could have been some influence by glacio-isostatic adjustments, causing our RSL
237 signals to deviate from the global sea level during MIS 5e (Stirling et al., 1998).
238 Around 129 ka, Sr/Ca rapidly increased, indicating the onset of the LBB flooding interval with the inferred RSL
239 above -6 m (Fig. 3). Absolute abundance of *G. menardii* per sample supports the inferred onset of the flooding
240 interval, since amounts of planktic foraminifera in the sample can be used to assess the relative accumulation of
241 platform-derived versus pelagic sediment particles (Slowey et al., 2002). Thus, after *G. menardii* repopulated the
242 (sub)tropical waters at the end of the penultimate glaciation (Bahr et al., 2011; Chabaud, 2016), its increased
243 absolute abundances are found around Bahamas between ~130-129 ka. This feature could be attributed to a
244 reduced input of fine-grained aragonite at times of partly flooded platform. Consequently, as the platform top
245 became completely submerged, established aragonite shedding gained over pelagic input, thereby reducing the
246 number of *G. menardii* per given sample. Our proxy records further suggest that the aragonite production on top
247 of the platform was abundant until late MIS 5e (unequivocally delimited by foraminiferal $\delta^{18}\text{O}$ and faunal data).
248 The drop in RSL below -6 m only during the terminal phase of MIS 5e (~117-115 ka on our timescale) is
249 corroborated by a coincident changeover in the aragonite content and an increase in absolute abundance of *G.*
250 *menardii*, further supporting the hypothesis that aragonite shedding was suppressed at that time, causing relative
251 enrichment in foraminiferal abundances.

252

253 **6.2 Deglacial changes in the vertical water mass structure**

254 Elevated proportions of thermocline-dwelling foraminifera *G. inflata* and *G. truncatulinoides* (dex) are found off
255 LBB during late MIS 6 and T2 (Fig. 4). To define mechanisms controlling the faunal assemblage, we look at $\delta^{18}\text{O}$
256 values in those foraminiferal species which document hydrographic changes across the upper water column, i.e.,
257 spanning from the uppermost mixed layer down to the permanent thermocline. The strongly reduced $\delta^{18}\text{O}$
258 gradients between surface-dwelling species *G. ruber* (white) and two thermocline-dwelling foraminifera *G.*
259 *truncatulinoides* (dex) and *G. inflata* during T2 and particularly during late MIS 6 could be interpreted in terms
260 of decreased water column stratification, a condition which is favored by thermocline-dwelling foraminifera (e.g.,
261 Mulitza et al., 1997). Specifically, for *G. truncatulinoides* (dex) this hypothesis is supported by its increased
262 abundance within the regions characterized by deep winter vertical mixing (Siccha and Kučera, 2017). Such
263 environmental preference may be explained by species ontogeny, given that *G. truncatulinoides* (dex) requires
264 reduced upper water column stratification to be able to complete its reproduction cycle with habitats ranging from
265 c. 400-600 m to near-surface depths; in well-stratified waters, however, reproduction of *G. truncatulinoides* (dex)

266 would be inhibited by a strong thermocline (Lohmann and Schweizer, 1990; Hilbrecht, 1996; Mulitza et al., 1997;
267 Schmuker and Schiebel, 2000).

268 To explain the inferred reduced upper water mass stratification during late MIS 6 and T2, sea surface
269 cooling/salinification and/or subsurface warming could be invoked (e.g., Zhang, 2007; Chiang et al., 2008).

270 While Mg/Ca-based temperature estimations during late MIS 6 so far reveal cold subsurface conditions for the
271 subtropical western North Atlantic (Bahr et al., 2011; 2013), it should be noted that species-specific signals (i.e.,
272 $\delta^{18}\text{O}$ values, Mg/Ca-ratios) could be complicated due to adaptation strategies of foraminifera, such as seasonal
273 shifts in the peak foraminiferal tests flux and/or habitat changes (Schmidt et al., 2006a, b; Cléroux et al., 2007;
274 Bahr et al., 2013; Jonkers and Kučera, 2015). However, further insights into the past fluctuations in seawater
275 temperature and salinity could be provided from the conspicuous millennial-scale oscillation found at 131 ka (Fig.
276 4) and associated with a shift towards lower surface-thermocline isotopic gradients (i.e., reduced stratification).

277 When compared to the abrupt increase in *G. ruber* (white) $\delta^{18}\text{O}$ values at 131 ka, which indicates sea surface
278 cooling or salinification, the isotopic response in thermocline-dwelling species remains rather muted. The latter
279 could be explained either by foraminiferal adaptation strategies, stable subsurface conditions and/or incorporation
280 of opposing signals during foraminiferal ontogenetic cycle that would mitigate the actual environmental change.

281 Regardless of the exact mechanism, there is a good coherence between $\delta^{18}\text{O}$ values in *G. ruber* (white) and relative
282 abundances of *G. inflata* and *G. truncatulinoides* (dex), suggesting a possible link between thermocline species
283 abundance and conditions occurring nearer to the sea surface (Mulitza et al., 1997; Jonkers and Kučera, 2017).

284 Specifically, steadily increasing upper water column stratification across glacial-interglacial transition could have
285 suppressed reproduction of *G. truncatulinoides* (dex) and *G. inflata*, while the short-term stratification reduction
286 at 131 ka may have promoted favorable conditions for the thermocline-dwelling species through sea surface
287 cooling and/or salinification.

288 It should be noted, however, that stratification is not a sole mechanism for explaining variability in the
289 thermocline-associated assemblage. Thus, while relative abundances of *G. inflata* become strongly reduced at the
290 onset of MIS 5e, there is no such response in the *G. truncatulinoides* (dex) proportions (Fig. 4). Whereas *G. inflata*
291 is generally regarded as subpolar to transitional species, preferring little seasonal variations in salinity (Hilbrecht,
292 1996), *G. truncatulinoides* (dex) was shown to dwell in warmer temperatures (Siccha and Kučera, 2017) and
293 occurs in small amounts also in the modern tropical Atlantic (Jentzen et al., 2018). However, an abrupt increase
294 in the latter species proportions during the sea surface cooling/salinification event at ~127 ka (see further below),

295 coupled with reduced upper water column stratification, supports the underlying “sea surface” control on the
296 general abundance of *G. truncatulinoides* (dex).

297 A southern position of the mean annual ITCZ during the penultimate (de)glaciation could be inferred based on
298 previous studies (Yarincik et al., 2000; Wang et al., 2004; Schmidt et al., 2006a; Carlson et al., 2008; Arbuszewski
299 et al., 2013; Bahr et al., 2013). By analogy with the modern atmospheric forcing in the region, a southern location
300 of the ITCZ could have caused enhanced upper water column mixing and evaporative cooling through intensified
301 trade winds (e.g., Wilson and Roberts, 1995). Acknowledging the fact that our study region lies too far north to
302 be influenced by changes in the winter position of the ITCZ (Ziegler et al., 2008) - this would be of primary
303 importance for modern-like winter-spring reproduction timing of *G. truncatulinoides* (dex) and *G. inflata* (Jonkers
304 and Kučera, 2015) - we suggest that a southern location of the mean annual position of the ITCZ during the
305 penultimate (de)glaciation could have facilitated favorable conditions for the latter species through generally
306 strong sea surface cooling/salinification in the subtropical North Atlantic.

307 Previous studies attributed increased Fe content in the Bahamas sediments to enhanced trade winds strength, given
308 that siliclastic inputs by other processes than wind transport are very limited (Roth and Reijmer, 2004).
309 Accordingly, elevated XRF-derived Fe counts in our record during T2 (Fig. 4) may support intensification of the
310 trade winds and possibly increased transport of Saharan dust at times of enhanced aridity over Northern Africa
311 (Muhs et al., 2007; Helmke et al., 2008). We, however, refrain from further interpretations of our XRF record due
312 to a variety of additional effects that may have influenced our Fe-record (e.g., diagenesis, change in sources and/or
313 properties of eolian inputs, sensitivity of the study region to atmospheric shifts).

314

315 **6.3 MIS 5e climate in the subtropics: orbital versus subpolar forcing**

316 Various environmental changes within the mixed layer (SST, SSS, nutrients) can account for proportional change
317 in different *Globigerinoides* species (Fig. 5). *G. sacculifer* - it makes up less than 10 % of the planktic
318 foraminiferal assemblage around the LBB today (Siccha and Kučera, 2017) - is abundant in the Caribbean Sea
319 and tropical Atlantic and commonly used as a tracer of tropical waters and geographical shifts of the ITCZ (Poore
320 et al., 2003; Vautravers et al., 2007). Also, *G. ruber* (pink) shows rather coherent abundance maxima in the tropics,
321 while no such affinity is observed for *G. ruber* (white) and *G. conglobatus* (Siccha and Kučera, 2017; Schiebel
322 and Hemleben, 2017). Therefore, fluctuations in relative abundances of *G. sacculifer* and *G. ruber* (pink) are
323 referred here as to represent a warm “tropical” end-member (Fig. 1b).

324 Relative abundances of the tropical foraminifera (here and further in the text *G. ruber* (pink) and *G. sacculifer*
325 calculated together) in our core suggest an early thermal maximum (between ~129 and 124 ka), which agrees well
326 with the recent compilation of global MIS 5e SST (Hoffman et al., 2017). The sea surface warming could be
327 related to a northward expansion of the Atlantic Warm Pool (Ziegler et al., 2008), in response to a northern
328 location of the mean annual position of the ITCZ. The latter shift in the atmospheric circulation is explained by
329 the particularly strong Northern Hemisphere insolation during early MIS 5e (Fig. 6), resulting in a cross-latitude
330 thermal gradient change, and in turn, forcing the ITCZ towards a warming (Northern) Hemisphere (Schneider et
331 al., 2014). A northern location of the mean annual position of the ITCZ during the first phase of the last interglacial
332 is supported by the XRF data from the Cariaco Basin, showing highest accumulation of the redox-sensitive
333 element molybdenum (Mo) during early MIS 5e (Fig. 6). At that latter location, high Mo content is found in
334 sediments deposited under anoxic conditions, occurring only during warm interstadial periods associated with a
335 northerly shifted ITCZ (Gibson and Peterson, 2014).

336 Further, our data reveal a millennial-scale cooling/salinification event at ~127 ka, characterized by decreased
337 proportions of the tropical foraminifera and elevated planktic $\delta^{18}\text{O}$ values (Fig. 6). That this abrupt cooling
338 characterized the entire upper water column at the onset of the event is indicated by the re-occurrence of cold-
339 water species *G. inflata* coincident with the brief positive excursions in $\delta^{18}\text{O}$ values in the shallow and
340 thermocline-dwelling foraminifera (Fig. 4). Simultaneously, the XRF record from the Cariaco Basin reveals a
341 stadial-like Mo-depleted (i.e., southward ITCZ shift) interval (Fig. 6). The close similarity between the tropical-
342 species record from the Bahamas and the XRF data from the Cariaco Basin supports the hypothesis that the annual
343 displacements of the ITCZ are also documented in our faunal counts. Thus, a southward shift in the mean annual
344 position of the ITCZ at ~127 ka could have restricted influence of the Atlantic Warm Pool in the Bahama region,
345 reducing SST and possibly increasing SSS, and in turn, affecting the foraminiferal assemblage. Moreover, because
346 the aforementioned abrupt climatic shift at ~127 ka cannot be reconciled with insolation changes, other forcing
347 factors at play during early MIS 5e should be considered. Studies from the low-latitude Atlantic reveal strong
348 coupling between the ITCZ position and the AMOC strength associated with millennial-scale climatic variability
349 (Rühlemann et al., 1999; Schmidt et al., 2006a; Carlson et al., 2008). In particular, model simulations and proxy
350 data suggest that freshwater inputs as well as sea-ice extent in the (sub)polar North Atlantic can affect the ITCZ
351 position through feedbacks on the thermohaline circulation and associated change in the cross-latitude heat
352 redistribution (e.g., Chiang et al., 2003; Broccoli et al., 2006; Gibson and Peterson, 2014).

353 It is well-established that the deepwater overflow from the Nordic Seas, which constitutes the deepest southward-
354 flowing branch of the AMOC today (e.g., Stahr and Sanford, 1999), strengthened (deepened) only during the
355 second phase of MIS 5e (at ~124 ka), and after the deglacial meltwater input into the region ceased (Hodell et al.,
356 2009; Barker et al., 2015). Nevertheless, several studies show that the deep-water ventilation and presumably the
357 AMOC abruptly recovered at the beginning of MIS 5e, at ~129 ka (Fig. 6), possibly linked to a deepened winter
358 convection in the Northwestern Atlantic (Adkins et al., 1997; Galaasen et al., 2014; Deaney et al., 2017).
359 Accordingly, the resumption of the AMOC could have added to a meridional redistribution of the incoming solar
360 heat, changing cross-latitude thermal gradient and, thus, contributing to the inferred “orbitally-driven”
361 northward ITCZ shift during early MIS 5e (see above). In turn, the millennial-scale climatic reversal between 127
362 and 126 ka could have been related to the known reductions of deep water ventilation (Galaasen et al., 2014;
363 Deaney et al., 2017), possibly attributed to a brief increase in the freshwater input into the subpolar North Atlantic
364 and accompanied by a regional sea surface cooling (Irvali et al., 2012; Zhuravleva et al., 2017b).

365 A corresponding cooling and freshening event, referred here and elsewhere as to a Younger Dryas-like event, is
366 captured in some high- and mid-latitude North Atlantic records (Sarnthein and Tiedemann, 1990; Bauch et al.,
367 2012; Irvali et al., 2012; Schwab et al., 2013; Govin et al., 2014; Jiménez-Amat and Zahn, 2015). Coherently with
368 the Younger Dryas-like cooling and the reduction (shallowing) in the North Atlantic Deep Water formation, an
369 increase in the Antarctic Bottom Water influence is revealed in the Southern Ocean sediments, arguing for the
370 existence of an “interglacial” bipolar seesaw (Hayes et al., 2014). The out-of-phase climatic relationship between
371 high northern and high southern latitudes, typical for the last glacial termination (Barker et al., 2009), could be
372 attributed to a strong sensitivity of the transitional climatic regime of early MIS 5e due to persistent high-latitude
373 freshening (i.e., continuing deglaciation, Fig. 6) and suppressed overturning in the Nordic Seas (Hodell et al.,
374 2009). This assumption seems of crucial importance as it might help explain a relatively “late” occurrence of the
375 Younger Dryas-like event during the last interglacial when compared to the actual Younger Dryas during the last
376 deglaciation (Bauch et al., 2012). The recognition of the transitional phase during early MIS 5e is not new, but
377 only few authors have pointed out its importance for understanding the last interglacial climatic evolution beyond
378 the subpolar regions (e.g., Govin et al., 2012; Schwab et al., 2013; Kandiano et al., 2014).

379 As insolation forcing decreased during late MIS 5e and the ITCZ gradually moved southward, the white variety
380 of *G. ruber* started to dominate the assemblage (Fig. 5), arguing for generally colder sea surface conditions in the
381 Bahama region. The inferred broad salinity tolerance of this species, also to neritic conditions (Bé and Tolderlund,
382 1971; Schmuker and Schiebel, 2002), was used in some studies to link high proportions of *G. ruber* (pink and

383 white varieties) with low SSS (Vautravers et al., 2007; Kandiano et al., 2012). The plots of the global distribution
384 pattern of *G. ruber* (white) and *G. ruber* (pink), however, suggest that when relative abundances of these two
385 species are approaching maximum values (40% and 10%, respectively), the SSSs would be higher for specimens
386 of the white variety of *G. ruber* (Hilbrecht, 1996). Therefore, the strongly dominating white versus pink *G. ruber*
387 variety observed in our records during late MIS 5e could be linked not only to decreasing SSTs, but also to
388 elevated SSSs.

389 In their study from the western STG, Bahr et al. (2013) also reconstruct sea surface salinification during late MIS
390 5e in response to enhanced wind stress at times of deteriorating high-latitude climate and increasing meridional
391 gradients. Accordingly, our isotopic and faunal data (note the abrupt decrease in *G. sacculifer* proportion at 120
392 ka; Fig. 5) suggest a pronounced climatic shift that could be attributed to the so-called “neoglaciation”, consistent
393 with the sea surface cooling in the western Nordic Seas and the Labrador Sea (Van Nieuwenhove et al., 2013;
394 Irvali et al., 2016) as well as with a renewed growth of terrestrial ice (Fronval and Jansen, 1997; Zhuravleva et
395 al., 2017a).

396

397 **7 Conclusions**

398 New faunal, isotopic and XRF evidence from the Bahama region were studied for past subtropical climatic
399 evolution, with special attention given to (1) the mechanisms controlling the planktic foraminiferal assemblage
400 and (2) the climatic feedbacks between low and high latitudes.

401 During late MIS 6 and glacial termination, strongly reduced $\delta^{18}\text{O}$ gradients between surface- and thermocline-
402 dwelling foraminifera suggest decreased water column stratification, which promoted high relative abundances
403 of *G. truncatulinoides* (dex) and *G. inflata*. The lowered upper water column stratification, in turn, could be a
404 result of sea surface cooling/salinification and intensified trade winds strength at times of the ITCZ being shifted
405 far to the south.

406 Computed together, relative abundances of the tropical foraminifera *G. sacculifer* and *G. ruber* (pink) agree well
407 with the published ITCZ-related Cariaco Basin record (Gibson and Peterson, 2014), suggesting a climatic
408 coupling between the regions. Based on these data, a northward/southward displacement of the mean annual ITCZ
409 position, in line with strong/weak Northern Hemisphere insolation, could be inferred for early/late MIS 5e.
410 Crucially, an abrupt Younger Dryas-like sea surface cooling/salinification event at ~127 ka intersected the early
411 MIS 5e warmth (between ~129 and 124 ka) and could be associated with a sudden southward displacement of the
412 ITCZ. This atmospheric shift, could be, in turn, related to a millennial-scale instability in the ocean overturning,

413 supporting a cross-latitude teleconnection that influenced the subtropical climate via ocean-atmospheric
414 forcing. These observations lead to an inference that the persistent ocean freshening in the high northern latitudes
415 (i.e., continuing deglaciation) and, therefore, unstable deep water overturning during early MIS 5e accounted for
416 a particularly sensitive climatic regime, associated with the abrupt warm-cold switches that could be traced across
417 various oceanic basins.

418

419 **Data availability**

420 All data is available in the online database PANGAEA ([doi.pangaea.de/10.1594/PANGAEA.893369](https://doi.org/10.1594/PANGAEA.893369)).

421

422 **Acknowledgments**

423 We wish to thank H. Lantzsch and J. J. G. Reijmer for providing us with the sediment core and data from core
424 MD99-2202, S. Fessler for performing measurements on stable isotopes, S. Müller and D. Garbe-Schönberg for
425 technical assistance during XRF scanning, J. Lübbers for her help with sample preparation, and E. Kandiano for
426 introduction into tropical foraminiferal assemblages. Comments by A. Bahr and one anonymous reviewer greatly
427 improved the manuscript. A. Z. acknowledges funding from German Research Foundation (DFG grant
428 BA1367/12-1).

429

430 **References**

- 431 Adkins, J. F., Boyle, E. A., Keigwin, L. and Cortijo, E.: Variability of the North Atlantic thermohaline circulation
432 during the last interglacial period, *Nature*, 390, 154, doi:10.1038/36540, 1997.
- 433 Arbuszewski, J. A., deMenocal, P. B., Cléroux, C., Bradtmiller, L., Mix, A.: Meridional shifts of the Atlantic
434 intertropical convergence zone since the Last Glacial Maximum, *Nature Geosci.* 6, 959, doi:
435 10.1038/ngeo1961, 2013.
- 436 Bahr, A., Nürnberg, D., Schönfeld, J., Garbe-Schönberg, D.: Hydrological variability in Florida Straits during
437 Marine Isotope Stage 5 cold events, *Paleoceanography*, 26, doi:10.1029/2010PA002015, 2011.
- 438 Bahr, A., Nürnberg, D., Karas, C. and Grützner, J.: Millennial-scale versus long-term dynamics in the surface and
439 subsurface of the western North Atlantic Subtropical Gyre during Marine Isotope Stage 5, *Glob. Planet.*
440 *Change*, 111, 77–87, doi:10.1016/j.gloplacha.2013.08.013, 2013.
- 441 Bahr, A., Jiménez-Espejo, F. J., Kolasinac, N., Grunert, P., Hernández-Molina F. J., Röhl U., Voelker A. H. L.,
442 Escutia C., Stow D. A. V., Hodell D. and Alvarez-Zarikian C. A.: Deciphering bottom current velocity

443 and paleoclimate signals from contourite deposits in the Gulf of Cádiz during the last 140 kyr: An
444 inorganic geochemical approach, *Geochem. Geophys. Geosyst.*, 15, 3145–3160,
445 doi:10.1002/2014GC005356, 2014.

446 Barker, S., Diz, P., Vautravers, M. J., Pike, J., Knorr, G., Hall, I. R. and Broecker, W. S.: Interhemispheric Atlantic
447 seesaw response during the last deglaciation, *Nature*, 457, 1097, doi:10.1038/nature07770, 2009.

448 Barker, S., Chen, J., Gong, X., Jonkers, L., Knorr, G., Thornalley, D.: Icebergs not the trigger for North Atlantic
449 cold events, *Nature* 520, 333, doi: 10.1038/nature14330, 2015.

450 Bauch, H. A., Kandiano, E. S. and Helmke, J. P.: Contrasting ocean changes between the subpolar and polar North
451 Atlantic during the past 135 ka, *Geophys. Res. Lett.*, 39, doi:10.1029/2012GL051800, 2012.

452 Bé, A. W. H. and Tolderlund, D. S.: Distribution and ecology of living planktonic foraminifera in surface waters
453 of the Atlantic and Indian Oceans, in: Funnel, B. and Riedel, W.R. (Eds.), *The Micropalaeontology of*
454 *Oceans*, Cambridge University Press, Cambridge, pp. 105–149, 1971.

455 Boli, H. M. and Saunders, J. B.: Oligocene to Holocene low latitude planktic foraminifera, in: Bolli, H.M.,
456 Saunders, J.B., Perch-Nielsen, K. (Eds.), *Plankton Stratigraphy*, Cambridge University Press, New York,
457 pp. 155–262, 1985.

458 Broccoli, A. J., Dahl, K. A., Stouffer, R. J.: Response of the ITCZ to Northern Hemisphere cooling, *Geophys.*
459 *Res. Lett.* 33, doi:10.1029/2005GL024546, 2006.

460 Carew, J. L. and Mylroie, J. E.: Quaternary tectonic stability of the Bahamian archipelago: evidence from fossil
461 coral reefs and flank margin caves, *Quat. Sci. Rev.*, 14, 145–153, doi:10.1016/0277-3791(94)00108-N,
462 1995.

463 Carew, J. L. and Mylroie, J. E.: Geology of the Bahamas, in: *Geology and Hydrogeology of Carbonate Islands,*
464 *Developments in Sedimentology*, 54, Elsevier Science, pp. 91–139, 1997.

465 Carlson, A. E., Oppo, D. W., Came, R. E., LeGrande, A. N., Keigwin, L. D. and Curry, W. B.: Subtropical Atlantic
466 salinity variability and Atlantic meridional circulation during the last deglaciation, *Geology*, 991–994,
467 doi:10.1130/G25080A, 2008.

468 Chabaud, L.: *Modèle stratigraphique et processus sédimentaires au Quaternaire sur deux pentes carbonatées des*
469 *Bahamas (leeward et windward)*, Doctoral dissertation, Université de Bordeaux, Français, 2016.

470 Chabaud, L., Ducassou, E., Tournadour, E., Mulder, T., Reijmer, J. J. G., Conesa, G., Giraudeau, J., Hanquiez,
471 V., Borgomano, J. and Ross, L.: Sedimentary processes determining the modern carbonate periplatform
472 drift of Little Bahama Bank, *Mar. Geol.*, 378, 213–229, doi:10.1016/j.margeo.2015.11.006, 2016.

473 Chang, P., Zhang, R., Hazeleger, W., Wen, C., Wan, X., Ji, L., Haarsma, R. J., Breugem, W.-P., Seidel, H.:
474 Oceanic link between abrupt changes in the North Atlantic Ocean and the African monsoon, *Nat.*
475 *Geosci.*, 1, 444, doi:10.1038/ngeo218, 2008.

476 Chiang, J. C. H., Biasutti, M., Battisti, D.S.: Sensitivity of the Atlantic Intertropical Convergence Zone to Last
477 Glacial Maximum boundary conditions, *Paleoceanography*, 18, doi:10.1029/2003PA000916, 2003.

478 Chiang, J. C. H., Cheng, W., Bitz, C.M.: Fast teleconnections to the tropical Atlantic sector from Atlantic
479 thermohaline adjustment, *Geophys. Res. Lett.*, 35, doi:10.1029/2008GL033292, 2008.

480 Cléroux, C., Cortijo, E., Duplessy, J. and Zahn, R.: Deep-dwelling foraminifera as thermocline temperature
481 recorders, *Geochem. Geophys. Geosyst.*, 8(4), doi:10.1029/2006GC001474, 2007.

482 Cortijo, E., Lehman, S., Keigwin, L., Chapman, M., Paillard, D. and Labeyrie, L.: Changes in Meridional
483 Temperature and Salinity Gradients in the North Atlantic Ocean (30°–72°N) during the Last Interglacial
484 Period, *Paleoceanography*, 14, 23–33, doi:10.1029/1998PA900004, 1999.

485 Deaney, E. L., Barker, S. and van de Flierdt, T.: Timing and nature of AMOC recovery across Termination 2 and
486 magnitude of deglacial CO₂ change, *Nat. Commun.*, 8, 14595, doi:10.1038/ncomms14595, 2017.

487 Droxler, A. W. and Schlager, W.: Glacial versus interglacial sedimentation rates and turbidite frequency in the
488 Bahamas, *Geology* 13, 799–802, 1985.

489 Dutton, A., Carlson, A. E., Long, A. J., Milne, G. A., Clark, P. U., DeConto, R., Horton, B. P., Rahmstorf, S. and
490 Raymo, M. E.: Sea-level rise due to polar ice-sheet mass loss during past warm periods, *Science*, 349,
491 doi:10.1126/science.aaa4019, 2015.

492 Ericson, D. B. and Wollin, G.: Pleistocene climates and chronology in deep-sea sediments, *Science*, 162(3859),
493 1227–1234, 1968.

494 Fronval, T. and Jansen, E.: Eemian and Early Weichselian (140–60 ka) Paleoceanography and paleoclimate in the
495 Nordic Seas with comparisons to Holocene conditions, *Paleoceanography*, 12, 443–462,
496 doi:10.1029/97PA00322, 1997.

497 Galaasen, E. V., Ninnemann, U. S., Irvali, N., Kleiven, H. (Kikki) F., Rosenthal, Y., Kissel, C. and Hodell, D. A.:
498 Rapid Reductions in North Atlantic Deep Water During the Peak of the Last Interglacial Period, *Science*,
499 343, 1129, doi:10.1126/science.1248667, 2014.

500 Gibson, K. A. and Peterson, L. C.: A 0.6 million year record of millennial-scale climate variability in the tropics,
501 *Geophys. Res. Lett.*, 41, 969–975, doi:10.1002/2013GL058846, 2014.

502 Govin, A., Braconnot, P., Capron, E., Cortijo, E., Duplessy, J.-C., Jansen, E., Labeyrie, L., Landais, A., Marti, O.,
503 Michel, E., Mosquet, E., Risebrobakken, B., Swingedouw, D. and Waelbroeck, C.: Persistent influence

504 of ice sheet melting on high northern latitude climate during the early Last Interglacial, *Clim. Past*, 8,
505 483–507, doi:10.5194/cp-8-483-2012, 2012.

506 Govin, A., Varma, V. and Prange, M.: Astronomically forced variations in western African rainfall (21°N–20°S)
507 during the Last Interglacial period, *Geophys. Res. Lett.*, 41, 2117–2125, doi:10.1002/2013GL058999,
508 2014.

509 Govin, A., Capron, E., Tzedakis, P. C., Verheyden, S., Ghaleb, B., Hillaire-Marcel, C., St-Onge, G., Stoner, J. S.,
510 Bassinot, F., Bazin, L., Blunier, T., Combourieu-Nebout, N., El Ouahabi, A., Genty, D., Gersonde, R.,
511 Jiménez-Amat, P., Landais, A., Martrat, B., Masson-Delmotte, V., Parrenin, F., Seidenkrantz, M.-S.,
512 Veres, D., Waelbroeck, C. and Zahn, R.: Sequence of events from the onset to the demise of the Last
513 Interglacial: Evaluating strengths and limitations of chronologies used in climatic archives, *Quat. Sci.*
514 *Rev.*, 129, 1–36, doi:10.1016/j.quascirev.2015.09.018, 2015.

515 Groeneveld, J. and Chiessi, C. M.: Mg/Ca of *Globorotalia inflata* as a recorder of permanent thermocline
516 temperatures in the South Atlantic, *Paleoceanography*, 26, doi:10.1029/2010PA001940, 2011.

517 Hayes, C. T., Martínez-García, A., Hasenfratz, A. P., Jaccard, S. L., Hodell, D. A., Sigman, D. M., Haug, G. H.
518 and Anderson, R. F.: A stagnation event in the deep South Atlantic during the last interglacial period,
519 *Science*, 346, 1514–1517, doi:10.1126/science.1256620, 2014.

520 Hearty, P. J. and Neumann, A. C.: Rapid sea level and climate change at the close of the Last Interglaciation (MIS
521 5e): evidence from the Bahama Islands, *Quat. Sci. Rev.*, 20, 1881–1895, doi:10.1016/S0277-
522 3791(01)00021-X, 2001.

523 Helmke, J. P., Bauch, H. A., Röhl, U. and Kandiano, E. S.: Uniform climate development between the subtropical
524 and subpolar Northeast Atlantic across marine isotope stage 11, *Clim. Past*, 4, 181–190, doi:10.5194/cp-
525 4-181-2008, 2008.

526 Hennekam, R. and de Lange, G., X-ray fluorescence core scanning of wet marine sediments: methods to improve
527 quality and reproducibility of high-resolution paleoenvironmental records, *Limnol. Oceanogr.*, 10, 991–
528 1003, doi:10.4319/lom.2012.10.991, 2012.

529 Hilbrecht, H.: Extant planktic foraminifera and the physical environment in the Atlantic and Indian Oceans: an
530 atlas based on Climap and Levitus (1982) data. *Mitteilungen aus dem Geologischen Institut der Eidgen.*
531 *Technischen Hochschule und der Universität Zürich, Neue Folge, Zürich*, 93 pp, 1996.

532 Hodell, D. A., Minth, E. K., Curtis, J. H., McCave, I. N., Hall, I. R., Channell, J. E. T., Xuan, C.: Surface and
533 deep-water hydrography on Gardar Drift (Iceland Basin) during the last interglacial period, *Earth Planet.*
534 *Sci. Lett.*, 288, 10–19, doi:10.1016/j.epsl.2009.08.040, 2009.

535 Hoffman, J. S., Clark, P. U., Parnell, A. C. and He, F.: Regional and global sea-surface temperatures during the
536 last interglaciation, *Science*, 355, 276, doi:10.1126/science.aai8464, 2017.

537 Irvah, N., Ninnemann, U. S., Galaasen, E. V., Rosenthal, Y., Kroon, D., Oppo, D. W., Kleiven, H. F., Darling, K.
538 F. and Kissel, C.: Rapid switches in subpolar North Atlantic hydrography and climate during the Last
539 Interglacial (MIS 5e), *Paleoceanography*, 27, PA2207, doi:10.1029/2011PA002244, 2012.

540 Irvah, N., Ninnemann, U. S., Kleiven, H. (Kikki) F., Galaasen, E. V., Morley, A. and Rosenthal, Y.: Evidence for
541 regional cooling, frontal advances, and East Greenland Ice Sheet changes during the demise of the last
542 interglacial, *Quat. Sci. Rev.*, 150, 184–199, doi:10.1016/j.quascirev.2016.08.029, 2016.

543 Jentzen, A., Schönfeld, J., Schiebel, R.: Assessment of the Effect of Increasing Temperature On the Ecology and
544 Assemblage Structure of Modern Planktic Foraminifers in the Caribbean and Surrounding Seas, *J.*
545 *Foraminiferal Res.*, 251–272, doi: 10.2113/gsjfr.48.3.251, 2018.

546 Jiménez-Amat, P. and Zahn, R.: Offset timing of climate oscillations during the last two glacial-interglacial
547 transitions connected with large-scale freshwater perturbation, *Paleoceanography*, 30, 768–788,
548 doi:10.1002/2014PA002710, 2015.

549 Johns, W. E., Townsend, T. L., Fratantoni, D. M. and Wilson, W. D.: On the Atlantic inflow to the Caribbean
550 Sea. *Deep Sea Research Part I: Oceanogr. Res. Pap.*, 49, 211–243. doi:10.1016/S0967-0637(01)00041-
551 3. 2002.

552 Jonkers, L. and Kučera, M.: Global analysis of seasonality in the shell flux of extant planktonic Foraminifera,
553 *Biogeosci.*, 12, 2207–2226, doi:10.5194/bg-12-2207-2015, 2015.

554 Kandiano, E. S., Bauch, H. A., Fahl, K., Helmke, J. P., Röhl, U., Pérez-Folgado, M. and Cacho, I.: The meridional
555 temperature gradient in the eastern North Atlantic during MIS 11 and its link to the ocean–atmosphere
556 system, *Palaeogeogr. Palaeoclimatol. Palaeoecol.*, 333–334, 24–39, doi:10.1016/j.palaeo.2012.03.005,
557 2012.

558 Kandiano, E. S., Bauch, H. A., Fahl, K., 2014. Last interglacial surface water structure in the western
559 Mediterranean (Balearic) Sea: Climatic variability and link between low and high latitudes, *Glob. Planet.*
560 *Change*, 123, 67–76, doi:10.1016/j.gloplacha.2014.10.004, 2014.

561 Lantzsch, H., Roth, S., Reijmer, J. J. G. and Kinkel, H.: Sea-level related resedimentation processes on the
562 northern slope of Little Bahama Bank (Middle Pleistocene to Holocene), *Sedimentology*, 54, 1307–1322,
563 doi:10.1111/j.1365-3091.2007.00882.x, 2007.

564 Laskar, J., Robutel, P., Joutel, F., Gastineau, M., Correia, A. C. M. and Levrard, B.: A long-term numerical
565 solution for the insolation quantities of the Earth, *Astron. Astrophys.*, 428, 261–285, doi:10.1051/0004-
566 6361:20041335, 2004.

567 Levitus, S., Antonov, J. I., Baranova, O. K., Boyer, T. P., Coleman, C. L., Garcia, H. E., Grodsky, A. I., Johnson,
568 D. R., Locarnini, R. A. and Mishonov, A. V.: The world ocean database, *Data Sci. J.*, 12, WDS229-
569 WDS234, 2013.

570 Lisiecki, L. E. and Stern, J. V.: Regional and global benthic $\delta^{18}\text{O}$ stacks for the last glacial cycle,
571 *Paleoceanography*, 31, 1368–1394, doi:10.1002/2016PA003002, 2016.

572 Lohmann, G. P. and Schweitzer, P. N.: *Globorotalia truncatulinoides*' Growth and chemistry as probes of the
573 past thermocline: 1. Shell size, *Paleoceanography*, 5, 55–75, doi:10.1029/PA005i001p00055, 2010.

574 Loulergue, L., Schilt, A., Spahni, R., Masson-Delmotte, V., Blunier, T., Lemieux, B., Barnola, J.-M., Raynaud,
575 D., Stocker, T. F. and Chappellaz, J.: Orbital and millennial-scale features of atmospheric CH_4 over the
576 past 800,000 years, *Nature*, 453, 383–386, doi:10.1038/nature06950, 2008.

577 Masson-Delmotte, V., Schulz, M., Abe-Ouchi, A., Beer, J., Ganopolski, A., González Rouco, J. F., Jansen, E.,
578 Lambeck, K., Luterbacher, J. and Naish, T.: Information from paleoclimate archives, in: Stocker, T. F.,
579 Qin, D., Plattner, G.-K., Tignor, M., Allen, S. K., Boschung, J., Nauels, A., Xia, Y., Bex, V., Midgley,
580 P.M. (Eds.), *Climate Change 2013: The Physical Science Basis. Contribution of Working Group I to the*
581 *Fifth Assessment Report of the Intergovernmental Panel on Climate Change*, pp. 383–464, 2013.

582 Morse, J. W. and MacKenzie, F. T.: *Geochemistry of sedimentary carbonates*, Elsevier, 1990.

583 Muhs, D. R., Budahn, J. R., Prospero, J. M., Carey, S. N.: Geochemical evidence for African dust inputs to soils
584 of western Atlantic islands: Barbados, the Bahamas, and Florida, *J. Geophys. Res.: Earth Surface*, 112,
585 doi:10.1029/2005JF0004452007, 2007.

586 Mulitza, S., Dürkoop, A., Hale, W., Wefer, G. and Niebler, H. S.: Planktonic foraminifera as recorders of past
587 surface-water stratification, *Geology*, 25(4), 335–338, doi:10.1130/0091-
588 7613(1997)025<0335:PFAROP>2.3.CO;2, 1997.

589 Neumann, A. C. and Land, L. S.: Lime mud deposition and calcareous algae in the Bight of Abaco, Bahamas; a
590 budget, *J. Sediment. Res.*, 45, 763–786, 1975.

591 NGRIP community members: High-resolution record of Northern Hemisphere climate extending into the last
592 interglacial period, *Nature*, 431, 147–151, doi:10.1038/nature02805, 2004.

593 Paillard, D., Labeyrie, L. and Yiou, P.: Macintosh Program performs time-series analysis, *Eos Trans, AGU* 77,
594 379–379, doi:10.1029/96EO00259, 1996.

595 Peterson, L. C. and Haug, G. H.: Variability in the mean latitude of the Atlantic Intertropical Convergence Zone
596 as recorded by riverine input of sediments to the Cariaco Basin (Venezuela), *Palaeogeogr.*
597 *Palaeoclimatol. Palaeoecol.*, 234, 97–113, doi:10.1016/j.palaeo.2005.10.021, 2006.

598 Poore, R. Z., Dowsett, H. J., Verardo, S., and Quinn, T. M.: Millennial- to century-scale variability in Gulf of
599 Mexico Holocene climate records, *Paleoceanography*, 18, doi:10.1029/2002PA000868, 2003.

600 Richter, T. O., van der Gaast, S., Koster, B., Vaars, A., Gieles, R., de Stigter, H. C., De Haas, H. and van Weering,
601 T. C. E.: The Avaatech XRF Core Scanner: technical description and applications to NE Atlantic
602 sediments, *Geol. Soc. London, Special Publications*, 267, 39, doi:10.1144/GSL.SP.2006.267.01.03,
603 2006.

604 Roth, S. and Reijmer, J. J. G.: Holocene Atlantic climate variations deduced from carbonate periplatform
605 sediments (leeward margin, Great Bahama Bank), *Paleoceanography*, 19, PA1003,
606 doi:10.1029/2003PA000885, 2004.

607 Roth, S. and Reijmer, J. J. G.: Holocene millennial to centennial carbonate cyclicity recorded in slope sediments
608 of the Great Bahama Bank and its climatic implications, *Sedimentology*, 52, 161–181,
609 doi:10.1111/j.1365-3091.2004.00684.x, 2005.

610 Rühlemann, C., Mulitza, S., Müller, P. J., Wefer, G. and Zahn, R.: Warming of the tropical Atlantic Ocean and
611 slowdown of thermohaline circulation during the last deglaciation, *Nature*, 402, 511,
612 doi:10.1038/990069, 1999.

613 Sarnthein, M. and Tiedemann, R.: Younger Dryas-style cooling events at glacial terminations I–VI at ODP site
614 658: Associated benthic $\delta^{13}\text{C}$ anomalies constrain meltwater hypothesis. *Paleoceanography and*
615 *Paleoclimatology*, 5, 1041–1055, doi: 10.1029/PA005i006p01041, 1990.

616 Schiebel, R. and Hemleben, C.: *Planktic Foraminifers in the Modern Ocean*, Springer, 2017.

617 Schlager, W., Reijmer, J. J. G. and Droxler, A.: Highstand Shedding of Carbonate Platforms, *J. Sedim. Res.*, 64B,
618 270–281, 1994.

619 Schlitzer, R.: *Ocean data view*, edited, 2012.

620 Schmidt, M. W., Vautravers, M. J. and Spero, H. J.: Rapid subtropical North Atlantic salinity oscillations across
621 Dansgaard–Oeschger cycles, *Nature*, 443, 561, doi:10.1038/nature05121, 2006a.

622 Schmidt, M. W., Vautravers, M. J. and Spero, H. J.: Western Caribbean sea surface temperatures during the late
623 Quaternary, *Geochem. Geophys. Geosyst.*, 7, doi:10.1029/2005GC000957, 2006b.

624 Schmitz, W. J. and McCartney, M. S.: On the North Atlantic Circulation, *Rev. Geophys.*, 31, 29–49,
625 doi:10.1029/92RG02583, 1993.

626 Schmitz, W. J. and Richardson, P. L.: On the sources of the Florida Current. *Deep Sea Res. Part A: Oceanogr.*
627 *Res. Pap.*, 38, S379–S409, doi:10.1016/S0198-0149(12)80018-5, 1991.

628 Schmuker, B. and Schiebel, R.: Planktic foraminifers and hydrography of the eastern and northern Caribbean Sea,
629 *Mar. Micropal.*, 46, 387–403, doi:10.1016/S0377-8398(02)00082-8, 2002.

630 Schneider, T., Bischoff, T., Haug, G. H.: Migrations and dynamics of the intertropical convergence zone, *Nature*,
631 513, 45, doi: 10.1038/nature13636, 2014.

632 Schwab, C., Kinkel, H., Weinelt, M. and Repschläger, J.: A coccolithophore based view on paleoenvironmental
633 changes in the open ocean mid-latitude North Atlantic between 130 and 48 ka BP with special emphasis
634 on MIS 5e, *Quat. Sci. Rev.*, 81, 35–47, doi:10.1016/j.quascirev.2013.09.021, 2013.

635 Siccha, M. and Kučera, M.: ForCenS, a curated database of planktonic foraminifera census counts in marine
636 surface sediment samples, *Sci. Data*, 4, 170109, 2017.

637 Slowey, N. C. and Curry, W. B.: Glacial-interglacial differences in circulation and carbon cycling within the upper
638 western North Atlantic, *Paleoceanography*, 10, 715–732, doi:10.1029/95PA01166, 1995.

639 Slowey, N. C., Wilber, R. J., Haddad, G. A. and Henderson, G. M.: Glacial-to-Holocene sedimentation on the
640 western slope of Great Bahama Bank, *Mar. Geol.*, 185, 165–176, doi:10.1016/S0025-3227(01)00295-X,
641 2002.

642 Stahr, F. R. and Sanford, T. B.: Transport and bottom boundary layer observations of the North Atlantic Deep
643 Western Boundary Current at the Blake Outer Ridge, *Deep Sea Res. Part II: Topical Studies in*
644 *Oceanography* 46, 205–243, doi:10.1016/S0967-0645(98)00101-5, 1999.

645 Stirling, C., Esat, T., Lambeck, K., McCulloch, M.: Timing and duration of the Last Interglacial: evidence for a
646 restricted interval of widespread coral reef growth, *Earth Planet. Sci. Lett.*, 160, 745–762,
647 doi:10.1016/S0012-821X(98)00125-3, 1998.

648 Stramma, L. and Schott, F.: The mean flow field of the tropical Atlantic Ocean. *Deep Sea Res. Part II: Trop. Stud.*,
649 *Oceanogr.*, 46, 279–303, doi:10.1016/S0967-0645(98)00109-X, 1999.

650 Tjallingii, R., Röhl, U., Kölling, M. and Bickert, T.: Influence of the water content on X-ray fluorescence core-
651 scanning measurements in soft marine sediments, *Geochem. Geophys. Geosyst.*, 8,
652 doi:10.1029/2006GC001393, 2007.

653 Van Nieuwenhove, N., Bauch, H. A. and Andruleit, H.: Multiproxy fossil comparison reveals contrasting surface
654 ocean conditions in the western Iceland Sea for the last two interglacials, *Palaeogeogr. Palaeoclimatol.*
655 *Palaeoecol.*, 370, 247–259, doi:10.1016/j.palaeo.2012.12.018, 2013.

656 Vautravers, M. J., Shackleton, N. J., Lopez-Martinez, C. and Grimalt, J. O.: Gulf Stream variability during marine
657 isotope stage 3, *Paleoceanography*, 19, PA2011, doi:10.1029/2003PA000966, 2004.

658 Vautravers, M. J., Bianchi, G. and Shackleton, N. J.: Subtropical NW Atlantic surface water variability during the
659 last interglacial, in: Sirocko, F., Claussen, M., Sánchez-Goni, M. F., Litt, T. (Eds.), *The Climate of Past*
660 *Interglacials*, *Developm. in Quat. Sci.*, Elsevier, pp. 289–303, doi:10.1016/S1571-0866(07)80045-5,
661 2007.

662 Vellinga, M. and Wood, R. A.: Global Climatic Impacts of a Collapse of the Atlantic Thermohaline Circulation,
663 *Clim. Change*, 54, 251–267, doi: 10.1023/A:1016168827653, 2002.

664 Wang, C. and Lee, S.: Atlantic warm pool, Caribbean low-level jet, and their potential impact on Atlantic
665 hurricanes, *Geophys. Res. Lett.*, 34, doi:10.1029/2006GL028579, 2007.

666 Wang, X., Auler, A. S., Edwards, R. L., Cheng, H., Cristalli, P. S., Smart, P. L., Richards, D. A., Shen, C.-C.:
667 Wet periods in northeastern Brazil over the past 210 kyr linked to distant climate anomalies, *Nature*, 432,
668 740, doi:10.1038/nature03067, 2004.

669 Williams, S. C.: *Stratigraphy, Facies Evolution and Diagenesis of Late Cenozoic Lime- stones and Dolomites,*
670 *Little Bahama Bank, Bahamas, Univ. Miami, Coral Gables FL, 1985.*

671 Wilson, P. A. and Roberts, H. H.: Density cascading: off-shelf sediment transport, evidence and implications,
672 *Bahama Banks, J. Sedim. Res.*, 65(1), 45-56, 1995.

673 Yarincik, K. M., Murray, R. W., Peterson, L. C.: Climatically sensitive eolian and hemipelagic deposition in the
674 Cariaco Basin, Venezuela, over the past 578,000 years: Results from Al/Ti and K/Al, *Paleoceanography*,
675 15, 210–228, doi:10.1029/1999PA900048, 2000.

676 Zhang, R.: Anticorrelated multidecadal variations between surface and subsurface tropical North Atlantic,
677 *Geophys. Res. Lett.*, 34, doi:10.1029/2007GL030225, 2007.

678 Zhuravleva, A., Bauch, H. A. and Spielhagen, R. F.: Atlantic water heat transfer through the Arctic Gateway
679 (Fram Strait) during the Last Interglacial, *Glob. Planet. Change*, 157, 232–243,
680 doi:10.1016/j.gloplacha.2017.09.005, 2017a.

681 Zhuravleva, A., Bauch, H.A. and Van Nieuwenhove, N.: Last Interglacial (MIS5e) hydrographic shifts linked to
682 meltwater discharges from the East Greenland margin, *Quat. Sci. Rev.*, 164, 95–109,
683 doi:10.1016/j.quascirev.2017.03.026, 2017b.

684 Ziegler, M., Nürnberg, D., Karas, C., Tiedemann, R. and Lourens, L. J.: Persistent summer expansion of the
685 Atlantic Warm Pool during glacial abrupt cold events, *Nature Geosci.*, 1, 601, doi:10.1038/ngeo277,
686 2008.

687

688

689 **Figure captions**

690 **Figure 1: Maps showing positions of investigated sediment records and oceanic/atmospheric circulation.**

691 (a) Simplified surface water circulation in the (sub)tropical North Atlantic and positions of investigated core
692 records: MD99-2202 (27°34.5' N, 78°57.9' W, 460 m water depth; *this study*), Ocean Drilling Program (ODP)
693 Site 1002 (10°42.7' N, 65°10.2' W, 893 m water depth; Gibson and Peterson, 2014), MD03-2664 (57°26.3' N,
694 48°36.4' W, 3442 m water depth, Galaasen et al., 2014) and PS1243 (69°22.3' N, 06°33.2' W, 2710 m water
695 depth, Bauch et al., 2012). (b) Relative abundances of the tropical foraminifera *G. sacculifer* and *G. ruber* (pink)
696 (Siccha and Kučera, 2017) and positions of the Intertropical Convergence Zone (ITCZ) during boreal winter and
697 summer. (c) Summer and winter hydrographic sections (as defined by the black line in b), showing temperature
698 and salinity obtained from the World Ocean Atlas (Levitus et al., 2013). Vertical bars denote calcification depths
699 of *G. ruber* (white) and *G. truncatulinoides* (dex). Note, that *G. truncatulinoides* (dex) reproduce in winter time
700 and due to its life cycle with changing habitats (as shown with arrows) accumulate signals from different water
701 depths. Maps are created using Ocean Data View (Schlitzer, 2016).

702

703 **Figure 2: The age model for MIS 5 in core MD99-2202.** The temporal framework is based on alignment of (b)
704 planktic $\delta^{18}\text{O}$ values (Lantsch et al., 2007) and (d) relative abundance record of *Globigerinoides* species with (a)
705 global benthic isotope stack LS16 (Lisiecki and Stern, 2016). (c) Aragonite content in black (Lantsch et al., 2007)
706 and normalized elemental intensities of Sr in magenta as well as (e) relative abundances of *G. menardii* are shown
707 to support the stratigraphic subdivision of MIS 5.

708

709 **Figure 3: XRF-scan results, sedimentological and foraminiferal data from core MD99-2202 for the period**
710 **140-100 ka.** (a) $\delta^{18}\text{O}$ values in *G. ruber* (white); (b) aragonite content; (a-b) is from Lantsch et al. (2007).
711 Normalized elemental intensities of (c) Sr, (e) Ca and (f) Cl, (d) Sr/Ca intensity ratio (truncated at 0.6) and (g)
712 absolute abundances of *G. menardii* per sample. Green bars denote core intervals with biased elemental intensities
713 due to high seawater content. The inferred platform flooding interval (see text) is consistent with the enhanced
714 production of Sr-rich aragonite needles and a RSL above -6 m (d). T2 refers to the position of the penultimate
715 deglaciation (Termination 2). Dashed vertical lines frame MIS 5e.

716

717 **Figure 4: Proxy records from core MD99-2202 over the last interglacial cycle.** (a) $\delta^{18}\text{O}$ values in *G. ruber*
718 (white) (Lantsch et al., 2007), (b) $\delta^{18}\text{O}$ values in *G. truncatulinoides* (dex) (in black) and *G. inflata* (in magenta),

719 (c-d) isotopic gradients between $\delta^{18}\text{O}$ values in *G. ruber* (white) and *G. truncatulinoides* (dex) and *G. ruber*
720 (white) and *G. inflata*, respectively, (e-f) relative abundances of *G. inflata* and *G. truncatulinoides* (dex),
721 respectively, (g) normalized Fe intensities. Also shown in (e) and (f) are modern relative foraminiferal abundances
722 (average value $\pm 1\sigma$) around Bahama Bank, computed using 7 nearest samples from Siccha and Kučera (2017)
723 database. Vertical blue bars represent periods of decreased water column stratification, discussed in the text.
724 Dashed vertical lines frame MIS 5e. T2 - Termination 2.

725

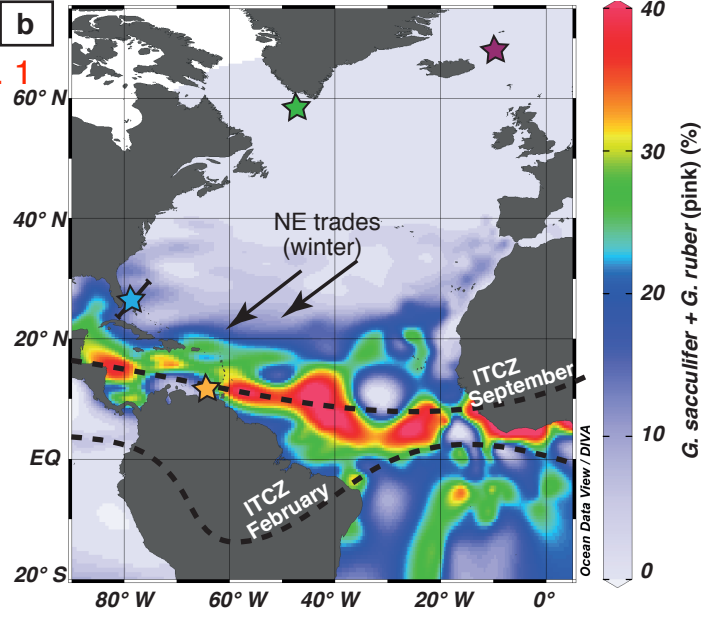
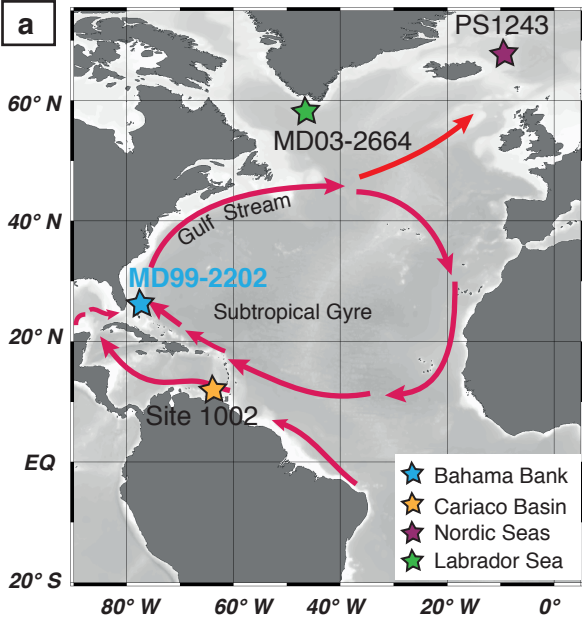
726 **Figure 5: Relative abundances of main *Globigerinoides* species in core MD99-2202 over the last interglacial**
727 **cycle. (a)** $\delta^{18}\text{O}$ values in *G. ruber* (white) (Lantzsich et al., 2007), relative abundances of (b) *G. sacculifer*, (c) *G.*
728 *ruber* (pink), (d) *G. conglobatus* and (e) *G. ruber* (white). Also shown in (b-e) are modern relative foraminiferal
729 abundances (average value $\pm 1\sigma$) around Bahama Bank, computed using 7 nearest samples from Siccha and Kučera
730 (2017) database. Dashed vertical lines frame MIS 5e. T2 - Termination 2.

731

732 **Figure 6: Comparison of proxy records from tropical, subtropical and subpolar North Atlantic over the**
733 **last interglacial cycle. (b)** $\delta^{18}\text{O}$ values in *G. ruber* (white) in core MD99-2202 (Lantzsich et al., 2007), (c) relative
734 abundances of the tropical species *G. sacculifer* and *G. ruber* (pink) in core MD99-2202, (d) molybdenum record
735 from ODP Site 1002 (Gibson and Peterson, 2014), (e) $\delta^{13}\text{C}$ values measured in benthic foraminifera from core
736 MD03-2664 (Galaasen et al., 2014, age model is from Zhuravleva et al., 2017b), (f) Ice-rafted debris in core
737 PS1243 (Bauch et al., 2012, age model is from Zhuravleva et al., 2017b). Also shown is (a) boreal summer
738 insolation (21 June, 30° N), computed with AnalySeries 2.0.8 (Paillard et al., 1996) using Laskar et al. (2004)
739 data. Shown in (c) are modern relative abundances of *G. sacculifer* and *G. ruber* (pink) (average value $\pm 1\sigma$)
740 around Bahama Bank, computed using 7 nearest samples from Siccha and Kučera (2017) database. The blue band
741 suggests correlation of events (Younger Dryas-like cooling) across tropical, subtropical and subpolar North
742 Atlantic (see text). Dashed vertical lines frame MIS 5e. T2 - Termination 2.

743

Fig. 1



c

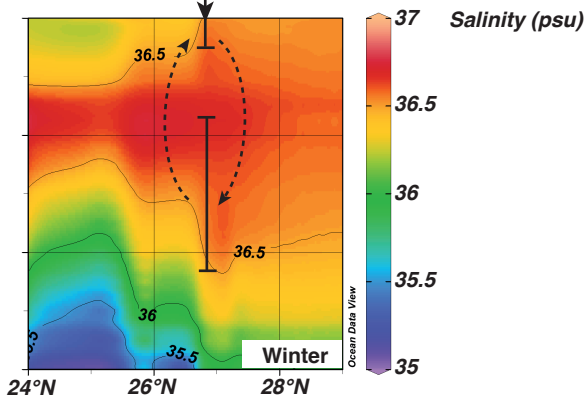
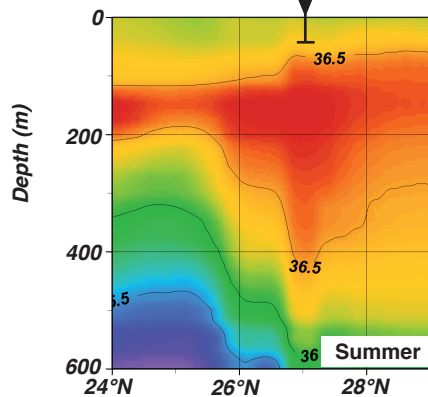
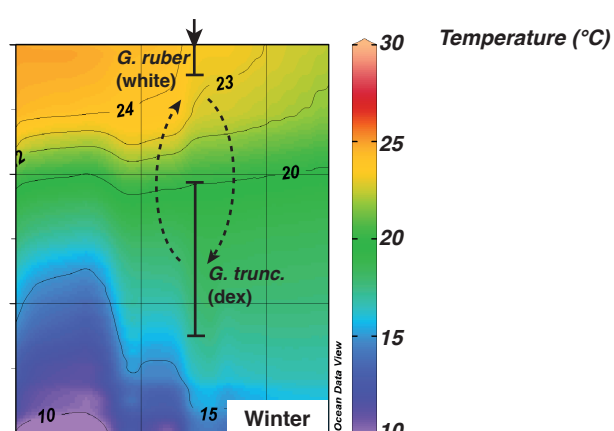
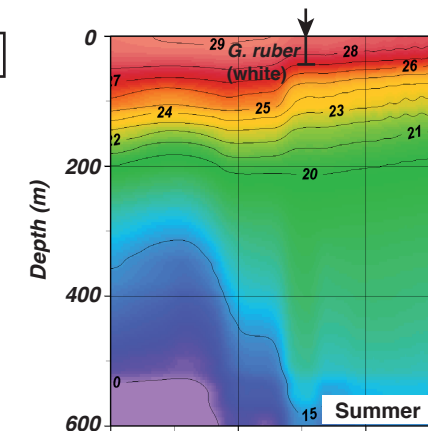


Fig. 2

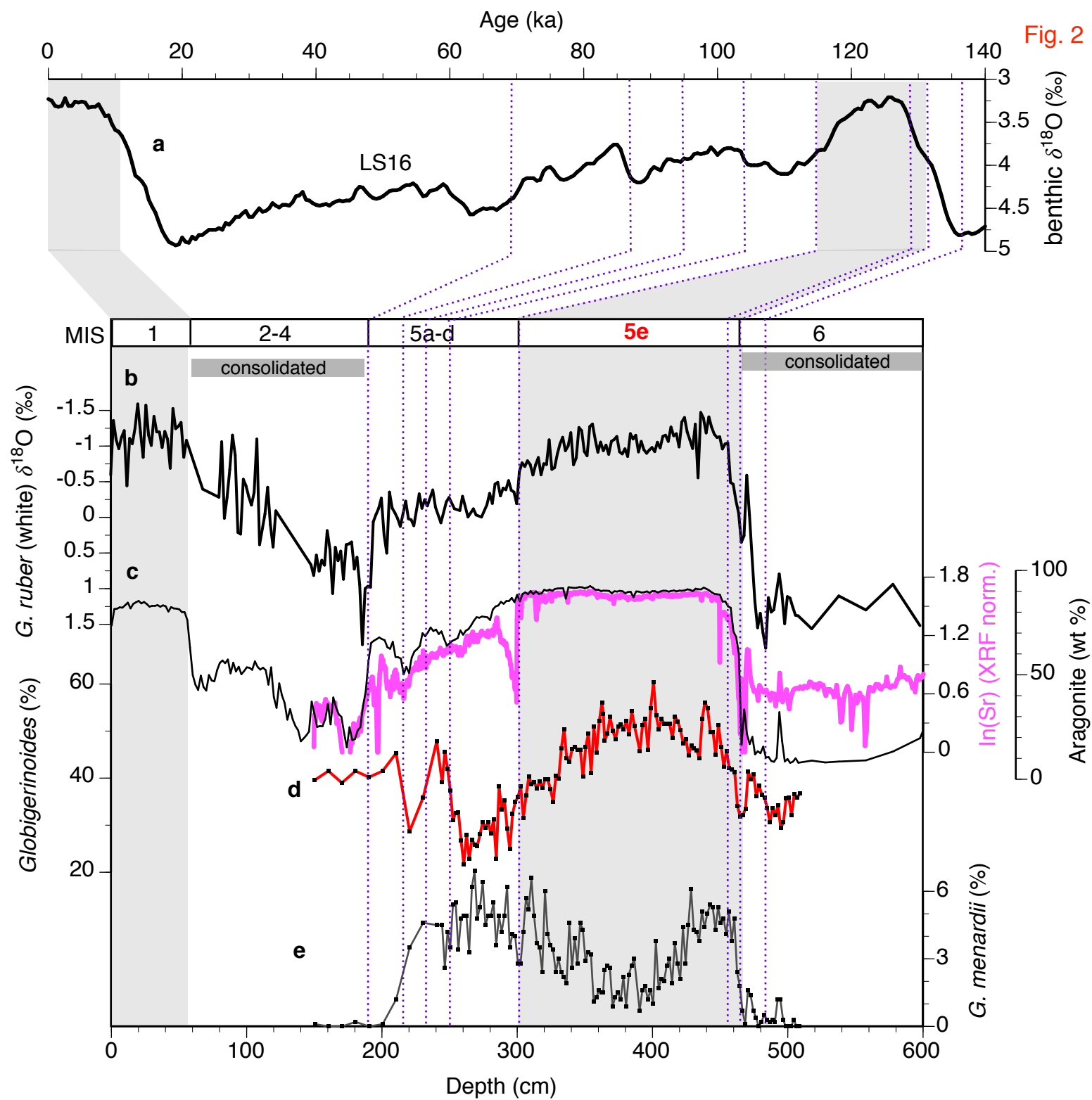
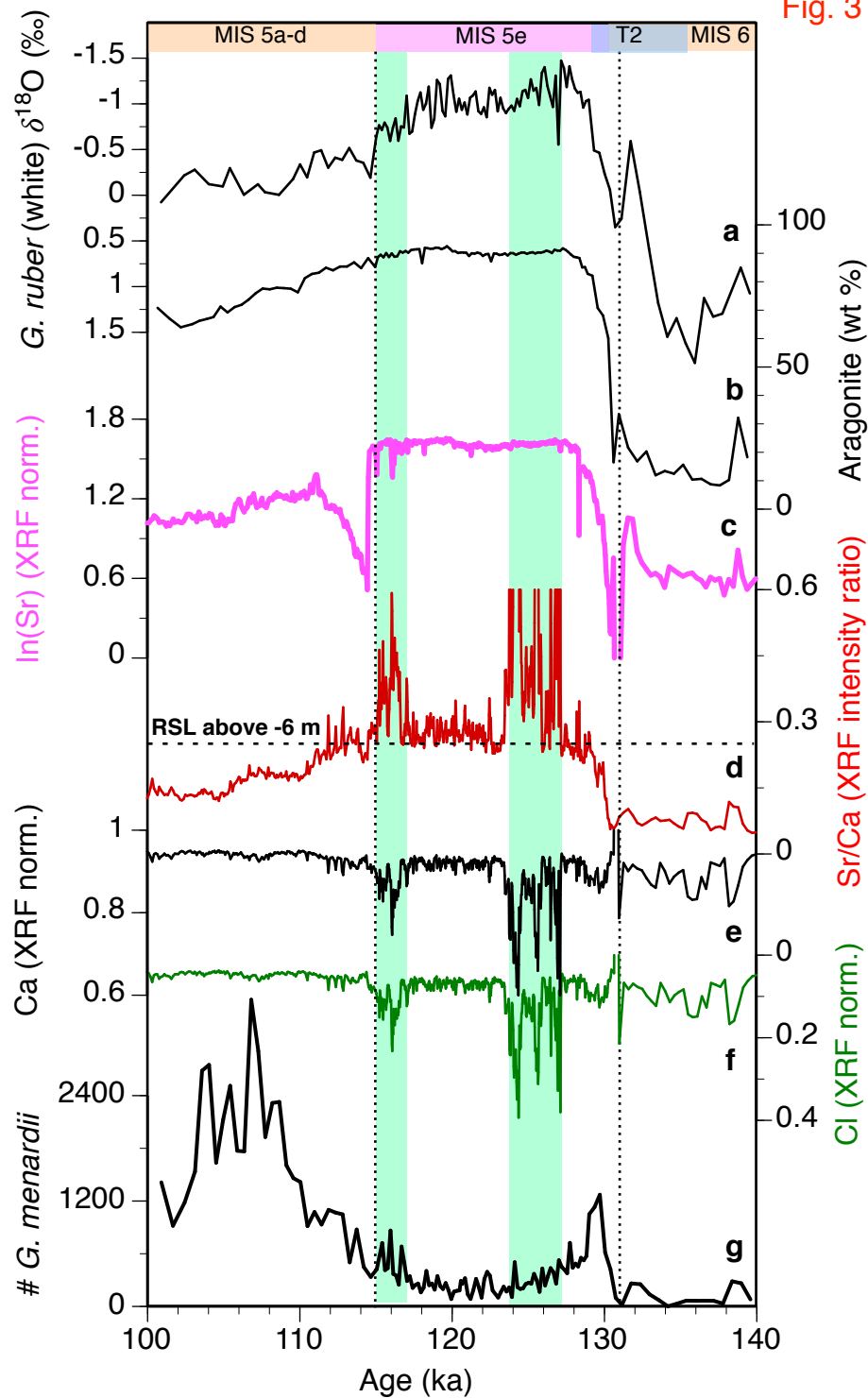


Fig. 3



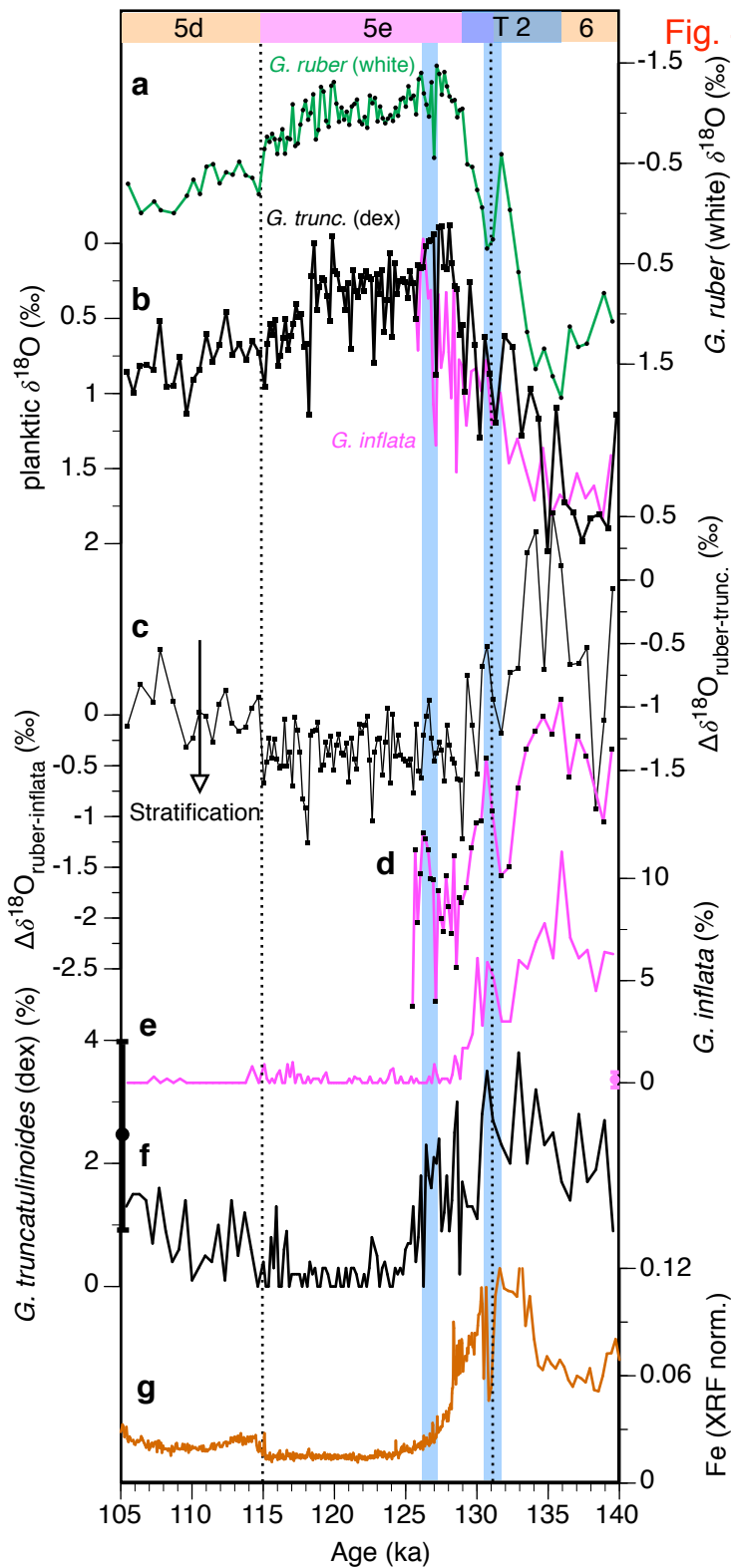


Fig. 5

